# Semiconductor steady state defect effective Fermi level and deep level transient spectroscopy depth profiling

Ken K. Chin† and Zimeng Cheng

Department of Physics and CNBM New Energy Materials Research Center, New Jersey Institute of Technology (NJIT), Newark, NJ 07102, USA

**Abstract:** The widely used deep level transient spectroscopy (DLTS) theory and data analysis usually assume that the defect level distribution is uniform through the depth of the depletion region of the n–p junction. In this work we introduce the concept of effective Fermi level of the steady state of semiconductor, by using which deep level transient spectroscopy depth profiling (DLTSDP) is proposed. Based on the relationship of its transition free energy level (TFEL) and the effective Fermi level, the rules of detectivity of the defect levels are listed. Computer simulation of DLTSDP is presented and compared with experimental data. The experimental DLTS data are compared with what the DLTSDP selection rules predicted. The agreement is satisfactory.

**Key words:** Fermi level; deep level transient spectroscopy; Schottky junction
**DOI:** 10.1088/1674-4926/37/9/092003 **PACS:** 78.40.Fy

## 1. Introduction

Current widely used deep level transient spectroscopy (DLTS) theory[1−3] assumes that the deep levels are spatially uniform through the depth of the depletion region of the semiconductor junction under investigation. Such an assumption of spatial uniformity is a reasonably good approximation for semiconductor n–p and Schottky junctions of well-controlled single-crystalline semiconductor materials, such as Si and III–V compounds used in electronics and optoelectronics. For thin film devices, such as CdTe and CIGS solar modules used in renewable energy industry worldwide, due to the requirement of low production cost, the distribution of defects through the n–p junction depth is highly non-uniform. For example, it is well known that CdS and CdTe intermix at the interface due to high processing temperature so that the $n^+$-CdS and p-CdTe interface is not sharp and the defects adjacent to and farther away from the interface are expected to be different[4−6]. In this work we present a comprehensive deep level transient spectroscopy depth profiling (DLTSDP) theory and its computer simulation results. The proposed rules of detectivity of defect levels by DLTS are compared with reported DLTS experimental results.

## 2. Transition free energy level (TFEL) $G$ and its occupation probability $f$

Assume that a point defect in a semiconductor has multiple transition levels between its charge states $q$ and $q'$, expressed as $(q/q')$. With $H^{(q)}$ as the enthalpy (often not distinguished from energy) and $g^{(q)}$ as the degeneracy of a charge state $q$, its (Gibbs) free energy is:

$$G^{(q)} = H^{(q)} - TS^{(q)} = H^{(q)} - kT\ln g^{(q)}, \tag{1}$$

where $S^{(q)}$ is the entropy of the charge state $q$, $k$ the Boltzmann constant, $T$ the temperature, and $kT = 0.0259$ eV under room temperature. If we consider a charge state of the aggregate of defects as a phase of the aggregate, then the transition from one charge state to another may be treated as if it is a phase transition[7]. Note that in phase transitions among the solid, liquid, and gas the different molecular interaction of each phase plays important roles. In the phase transition between the point defect charge states the interaction among defects is usually negligible due to its low density. It occurs when the Fermi level of the host semiconductor is equal to the transition free energy level, at which the free energies of the two charge states are equal. Note that Helmholtz free energy under constant volume and Gibbs free energy under constant pressure are usually not distinguished for condensed matter. Dependence of the defect's free energy of its various charge states on the Fermi level of the host semiconductor is[8, 9]:

$$\begin{cases} G^{(-)}(E_{\rm F}) = \Delta G_{\rm o}^{(-)} - 2E_{\rm F}, \\ G^{(-)}(E_{\rm F}) = \Delta G_{\rm o}^{(-)} - E_{\rm F}, \\ G^{(0)}(E_{\rm F}) = \Delta G_{\rm o}^{(0)}, \quad \text{independent of } E_{\rm F}, \\ G^{(+)}(E_{\rm F}) = \Delta G_{\rm o}^{(+)} + E_{\rm F}, \\ G^{(++)}(E_{\rm F}) = \Delta G_{\rm o}^{(++)} + 2E_{\rm F}, \end{cases} \tag{2}$$

where $\Delta G_{\rm o}^{(q)}$ is the free energy of formation of the defect with charge $q$, and $E_{\rm F}$ the Fermi level. Thus, the free energy level of the transition from charge state $q$ to $q'$, with $q' = q - 1$, is:

$$G^{(q/q')} = \Delta G_o^{(q')} - \Delta G_o^{(q)} = H^{(q/q')} - kT\ln\frac{g^{(q')}}{g^{(q)}}. \tag{3}$$

By introducing the transition free energy level (TFEL) $G$[7] to replace the transition energy level (TEL) $E$ and its degeneracy $g$, the electron occupation probability of the defect under thermodynamic equilibrium is simplified as:

$$f = \frac{1}{1 + \exp\frac{G - E_{\rm F}}{kT}}. \tag{4}$$

† Corresponding author. Email: chin@njit.edu
Received 7 October 2015, revised manuscript received 13 April 2016

Note that the degeneracy involved in $G$ may be far more than the symmetry induced $g_A = 4$ for acceptor and $g_D = \frac{1}{2}$ for widely used tetrahedral semiconductors, such as Si, GaAs, and CdTe[10]. According to the theory of micro-excitation, the phonon degeneracy induced $kT\ln g$, far greater than that due to symmetry, is proportional to the TEL[11, 12]. The steady-state occupation probability of TFEL $G$, either single donor or single acceptor (the multilevel defects are to be discussed in another work), is[3, 13–18]:

Single donor $f^{(+/0)}$:

$$\begin{cases} f^{(+)} = 1 - f = \dfrac{c_\mathrm{p} + e_\mathrm{n}}{c_\mathrm{n} + e_\mathrm{n} + c_\mathrm{p} + e_\mathrm{p}}, & \text{Empty}, \\ f^{(0)} = f = \dfrac{c_\mathrm{n} + e_\mathrm{p}}{c_\mathrm{n} + e_\mathrm{n} + c_\mathrm{p} + e_\mathrm{p}}, & \text{Occupied}, \end{cases} \tag{5a}$$

Single acceptor $f^{(0/-)}$:

$$\begin{cases} f^{(0)} = (1 - f) = \dfrac{c_\mathrm{p} + e_\mathrm{n}}{c_\mathrm{n} + e_\mathrm{n} + c_\mathrm{p} + e_\mathrm{p}}, & \text{Empty}, \\ f^{(-)} = f = \dfrac{c_\mathrm{n} + e_\mathrm{p}}{c_\mathrm{n} + e_\mathrm{n} + c_\mathrm{p} + e_\mathrm{p}}, & \text{Occupied}, \end{cases} \tag{5b}$$

where

$$\begin{cases} c_\mathrm{n} = \sigma_\mathrm{n} v_\mathrm{n} n, \\ c_\mathrm{p} = \sigma_\mathrm{p} v_\mathrm{p} p, \\ e_\mathrm{n} = \sigma_\mathrm{n} v_\mathrm{n} n^*, \\ e_\mathrm{p} = \sigma_\mathrm{p} v_\mathrm{p} p^*. \end{cases} \tag{6}$$

In Equation (6), $c_\mathrm{n}$, $c_\mathrm{p}$, $e_\mathrm{n}$, and $e_\mathrm{p}$ are the defect TFEL's capture rate of electron, of hole, and the emission rate of electron and of hole, respectively. The electron density $n$ and the hole density $p$, as well as $n^*$ and $p^*$ are determined by:

$$\begin{cases} n = N_\mathrm{C} \exp \frac{E_\mathrm{Fn} - E_\mathrm{C}}{kT} = n_\mathrm{i} \exp \frac{E_\mathrm{Fn} - E_\mathrm{i}}{kT}, \\ p = N_\mathrm{V} \exp \frac{E_\mathrm{V} - E_\mathrm{Fp}}{kT} = n_\mathrm{i} \exp \frac{E_\mathrm{i} - E_\mathrm{Fp}}{kT}, \\ n^* = N_\mathrm{C} \exp \frac{G - E_\mathrm{C}}{kT} = n_\mathrm{i} \exp \frac{G - E_\mathrm{i}}{kT}, \\ p^* = N_\mathrm{V} \exp \frac{E_\mathrm{V} - G}{kT} = n_\mathrm{i} \exp \frac{E_\mathrm{i} - G}{kT}, \end{cases} \tag{7}$$

where $E_\mathrm{i}$ is the intrinsic Fermi level, $E_\mathrm{C}$, $E_\mathrm{V}$, $E_\mathrm{Fn}$ and $E_\mathrm{Fp}$ the conduction band minimum, valence band maximum, quasi Fermi level of electron and of hole, respectively. $n_\mathrm{i}$, $N_\mathrm{C}$, and $N_\mathrm{V}$ are the intrinsic carrier density, effective density of states in the conduction and valence band, respectively. It is interesting to note that $n^*$ is as if it were $n$, but with $E_\mathrm{Fn}$ replaced by the defect's TFEL $G$; and similarly, $p^*$ is $p$ with $E_\mathrm{Fp}$ replaced by $G$. Such a simple relationship does not exist if $H$ and $g$ were used instead of $G$[7].

Defining $\alpha$, the geometric average of the defect level's capacity of capturing electron and hole, as well as $\beta$, the ratio of the capacity of electron capture versus that of hole capture:

$$\alpha = \sqrt{\sigma_\mathrm{n} v_\mathrm{n} \sigma_\mathrm{p} v_\mathrm{p}}, \tag{8}$$

$$\beta = \sqrt{\frac{\sigma_\mathrm{n} v_\mathrm{n}}{\sigma_\mathrm{p} v_\mathrm{p}}}, \tag{9}$$

where $\sigma_\mathrm{n}$, $\sigma_\mathrm{p}$, $v_\mathrm{n}$, and $v_\mathrm{p}$ are the defect level's cross section of capturing electrons and holes, the average thermal velocity of the electron and of the hole, respectively. Due to Coulomb interaction between the defect and the carrier, we have $\beta \gg 1$ for donor and $\beta \ll 1$ for acceptor [7].

Defining:

$$\beta = \exp \frac{\Delta E_\beta}{kT}, \tag{10}$$

and substituting Equations (6)–(10) to Equation (5), we have:

$$\begin{aligned} f = & \left[ \exp \frac{E_\mathrm{Fn} - (E_\mathrm{i} - \Delta E_\beta)}{kT} + \exp \frac{(E_\mathrm{i} - \Delta E_\beta) - G}{kT} \right] \\ & \times \left[ \exp \frac{E_\mathrm{Fn} - (E_\mathrm{i} - \Delta E_\beta)}{kT} + \exp \frac{G - (E_\mathrm{i} - \Delta E_\beta)}{kT} \right. \\ & \left. + \exp \frac{(E_\mathrm{i} - \Delta E_\beta) - E_\mathrm{Fp}}{kT} + \exp \frac{(E_\mathrm{i} - \Delta E_\beta) - G}{kT} \right]^{-1}. \end{aligned} \tag{11}$$

Thus, the effect of $\beta$ on steady state occupation probability of the TFEL is to change the intrinsic Fermi level from $E_\mathrm{i}$ to $E_\mathrm{i} - \Delta E_\beta$. $E_\mathrm{i}$ is lowered by $\Delta E_\beta (\Delta E_\beta > 0)$ for donor, and raised by $\Delta E_\beta (\Delta E_\beta < 0)$.

## 3. Definition of steady state effective Fermi energy $E_\mathrm{F}^\mathrm{eff}$ for the defect TFEL

We define the steady state effective Fermi energy $E_\mathrm{F}^\mathrm{eff}$[19, 20]. If the TFEL's $G = E_\mathrm{F}^\mathrm{eff}$, its occupation probability is $\frac{1}{2}$. $E_\mathrm{F}^\mathrm{eff}$ is calculated[19, 20] from the equation:

$$\begin{aligned} & \exp \frac{E_\mathrm{Fn} - (E_\mathrm{i} - \Delta E_\beta)}{kT} + \exp \frac{(E_\mathrm{i} - \Delta E_\beta) - E_\mathrm{F}^\mathrm{eff}}{kT} \\ & = \exp \frac{(E_\mathrm{i} - \Delta E_\beta) - E_\mathrm{Fp}}{kT} + \exp \frac{E_\mathrm{F}^\mathrm{eff} - (E_\mathrm{i} - \Delta E_\beta)}{kT}. \end{aligned} \tag{12}$$

From Equation (12) we can derive an explicit analytical expression of $E_\mathrm{F}^\mathrm{eff}$ as a function of the quasi-Fermi levels $E_\mathrm{Fp}$ and $E_\mathrm{Fn}$, and $\Delta E_\beta$, which characterizes the TFEL's charge states, and to which the effective Fermi energy is referred to:

$$\begin{aligned} E_\mathrm{F}^\mathrm{eff} = & E_\mathrm{i} - \Delta E_\beta \\ & + kT \sinh^{-1} \left[ \exp \frac{qV}{2kT} \sinh \frac{\frac{E_\mathrm{Fn} + E_\mathrm{Fp}}{2} - (E_\mathrm{i} - \Delta E_\beta)}{kT} \right], \end{aligned} \tag{13}$$

where $q$ is the electron charge, and $V = \frac{E_\mathrm{Fn} - E_\mathrm{Fp}}{q}$ the bias voltage of the n–p junction. The steady state occupation probability of TFEL $G$ is:

$$f = \begin{cases} 1, & G \ll E_\mathrm{F}^\mathrm{eff}, \\ \dfrac{1}{2}, & G = E_\mathrm{F}^\mathrm{eff}, \\ 0, & G \gg E_\mathrm{F}^\mathrm{eff}. \end{cases} \tag{14}$$

The role of steady state effective Fermi level $E_\mathrm{F}^\mathrm{eff}$ is the same as equilibrium state Fermi level. $E_\mathrm{F}$ as shown in Equation (4).

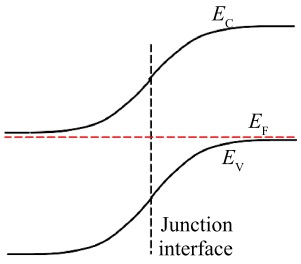


Figure 1. Symmetric n/p junction in equilibrium with $V = 0$.

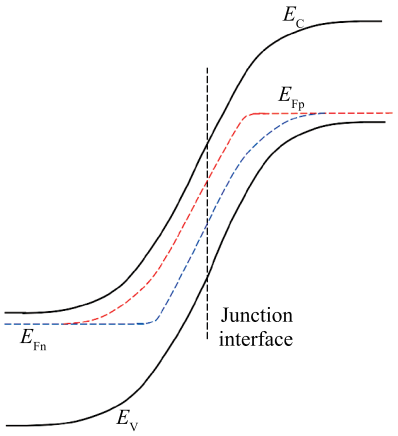


Figure 2. Symmetric n/p junction with reverse bias $V = -3$ V. Note that both the Shockley and Shockley-Read-Hall diode theories[10] assume that the quasi Fermi levels are flat across the junction depletion region. Such an assumption is only approximately valid when the bias voltage is smaller than the band gap energy. Theory as well as computer simulation[21] show that under large bias voltage, as in the case of DLTS, the quasi Fermi levels do not keep constant through the depletion region. They mostly follow the band bending across the depletion or space charge or region as shown in Figures 2 and 4.

## 4. Steady state standard and flattened band bending diagrams

Band bending profile of the depletion region — also called space charge region (SCR) — is the electron's potential distribution $\Psi(x)$, which can be calculated from the Poisson equation:

$$\frac{\varepsilon}{q}\frac{d^2\Psi(x)}{dx^2} = p - n + \sum N_D^+ - \sum N_A^-, \qquad (15)$$

where $\varepsilon$ is the permittivity of the semiconductor, $N_D^+$ and $N_A^-$ the ionized donor and acceptor concentration, respectively. $\Sigma$ sums over all the donor and acceptor levels. The free carrier electron and hole density $n$ and $p$ are determined by the material's quasi-Fermi levels of electron and hole $E_{Fn}$ and $E_{Fp}$, as shown in Equation (7), respectively. The concentration of ionized donor and acceptor are calculated using the occupation probability of Equation (4) for equilibrium state and Equation (5) for steady state.

In this work we consider two extreme special cases: the symmetric n/p junction (Figures 1 and 2) and the abrupt $n^+$/p junction (Figures 3 and 4). Take the $n^+$-CdS / p-CdTe solar cell (Figures 3 and 4) as an example. We define $x = 0$ at the interface, and the conduction band minimum or electron affinity of $n^+$-CdS, the band bending of which is negligible, being $E_C =$

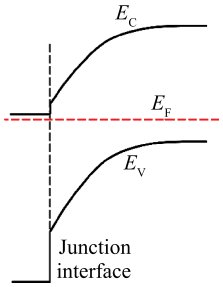


Figure 3. Abrupt $n^+$/p junction in equilibrium with $V = 0$.

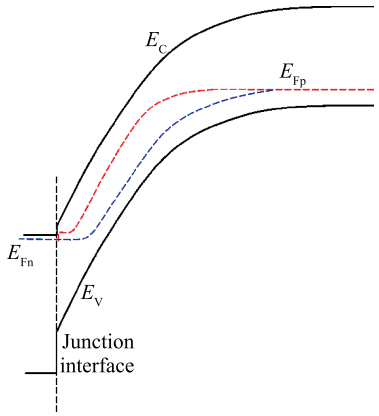


Figure 4. Abrupt $n^+$/p junction with reverse bias $V = -3$ V.

0. Thus, the boundary conditions of the space charge induced potential in p-CdTe is:

$$\begin{cases} \Psi(0) = \Delta E_C, \\ \Psi(\infty) = \Delta E_C + q(V_{bi} - V), \end{cases} \qquad (16)$$

where $\Delta E_C = 0.1$ eV is the band offset of the $n^+$-CdS / p-CdTe interface, and:

$$qV_{bi} = E_G - \Delta e_n - \Delta E_C - \Delta e_p \qquad (17)$$

is the built-in or flat band condition. $\Delta e_n \sim 0.1$ eV ($n \sim 10^{17}$ cm$^{-3}$), and $\Delta e_p \sim 0.3$ eV ($p \sim 10^{14}$ cm$^{-3}$), as shown in Figure 3.

The spatial dependence of the various energy levels are the valence band maximum (VBM) $E_V(x) = \Psi(x)$ conduction band minimum (CBM) $E_C(x) = E_C + \Psi(x)$, intrinsic Fermi level $E_i(x) = E_i + \Psi(x)$, and $G(x) = G + \Psi(x)$ of all the defect TFEL, while $E_{Fp} = \Delta e_p = 0.313$ eV and $E_{Fn} = qV + E_{Fp}$ are constants. Figures 1 and 2 are the widely used standard band bending diagrams of a symmetric homogeneous n–p junction under 0 bias and –3 V bias, respectively. Figures 3 and 4 are the counterparts of Figures 1 and 2 of an abrupt $n^+$-CdS / p-CdTe heterojunction solar cell. Figures 5–8 are the flattened band diagrams of the standard band bending diagrams as shown in Figure 1–4. In the flattened band bend diagrams a spatial potential energy $-\Psi(x)$ is added onto all the energy levels. As a result, in Figures 5–8, the Fermi level $E_F$ and quasi Fermi level $E_{Fn}$ and $E_{Fp}$ are curves, while all the other energy levels are constants. The advantage of flattened band diagrams[19] is the clear relationship of $G$ with respect to $E_V$, $E_C$, and $E_i$.

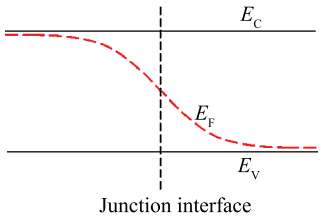


Figure 5. Flattened band diagram of symmetric n/p junction in equilibrium with $V = 0$.

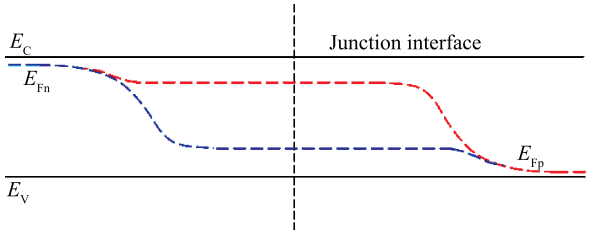


Figure 6. Flattened band diagram of symmetric n/p junction with reverse bias $V = -3$ V.

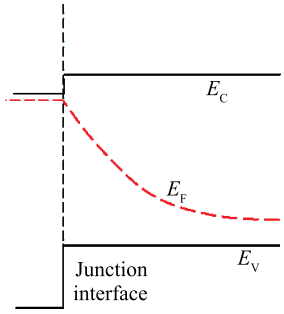


Figure 7. Flattened band diagram of abrupt $n^+$/p junction in equilibrium $V = 0$.

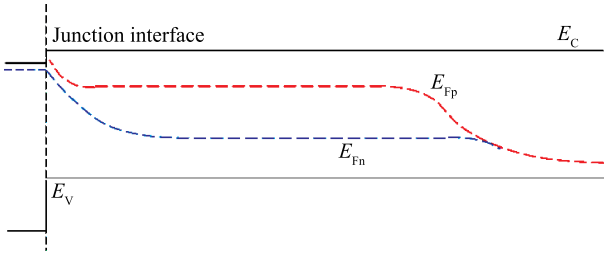


Figure 8. Flattened band diagram of abrupt $n^+$/p junction with reverse bias $V = -3$ V.

## 5. Selection rules of carrier emission of defect levels and theory of deep level transient spectroscopy depth profiling (DLTSDP)

In DLTS, a semiconductor junction is first biased at around 0 V at low temperature to reach steady state 1 (or quasi steady state if the first bias pulse lasts a short time). It is followed by an abrupt application of a negative bias voltage (from –2 to –5 V) for the sample's temperature to go up gradually and reach steady state 2 (Figure 9, for symmetric n/p junction with the defect TFEL's $\beta = 1$). Compared to the application of

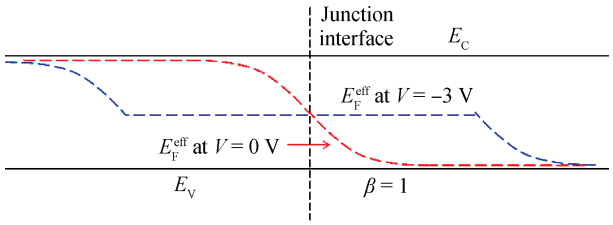


Figure 9. Effective Fermi level of symmetric n/p junction steady state 1 ($V = 0$) and 2 ($V = -3$ V), $\beta = 1$.

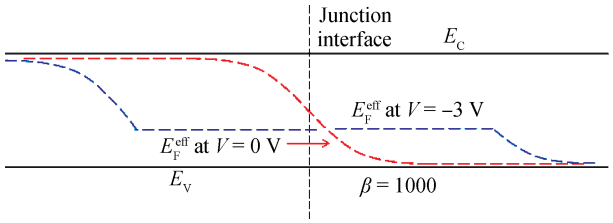


Figure 10. Effective Fermi level of symmetric n/p junction steady state 1 ($V = 0$) and 2 ($V = -3$ V), $\beta = 1000$.

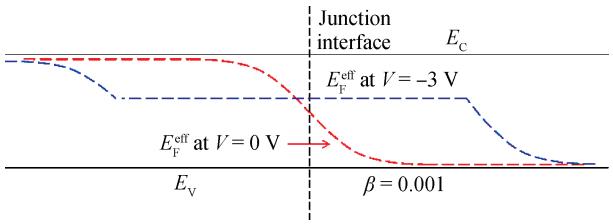


Figure 11. Effective Fermi level of symmetric n/p junction steady state 1 ($V = 0$) and 2 ($V = -3$ V), $\beta = 0.001$.

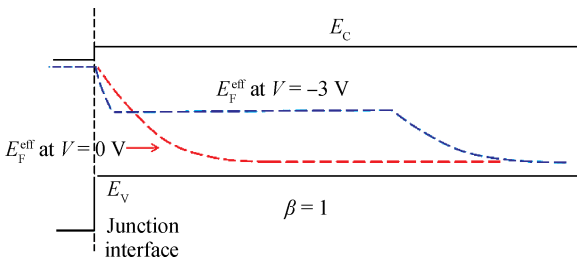


Figure 12. Effective Fermi level of $n^+$/p junction steady state 1 ($V = 0$) and 2 ($V = -3$ V), $\beta = 1$.

junction bias voltage, the charging and discharging of defect levels in the SCR of the junction is far slower. During the transient process from steady state 1 to steady state 2, the defects in the SCR may emit or capture free electric carriers. The variation of charges on the defects is characterized by the junction capacitance. By analyzing the capacitance measurement data, we may acquire the characteristics of the junction defects. For the SCR defect to capture or emit a carrier, it must change its occupation probability, which is as shown in Equation (14).

Figures 9–11 depict the effective Fermi level for the symmetric n–p homojunction under 0 or –3 V bias for $\beta = 1$, 1000 (donor or double donor), and 0.001 (acceptor or double acceptor), respectively. Figures 12–14 for the abrupt $n^+$-CdS/p-CdTe heterojunction, is the counterpart of Figures 9–11.

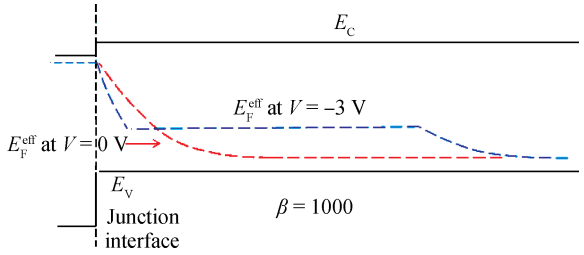


Figure 13. Effective Fermi level of $n^+/p$ junction steady state 1 ($V = 0$) and 2 ($V = -3$ V), $\beta = 1000$.

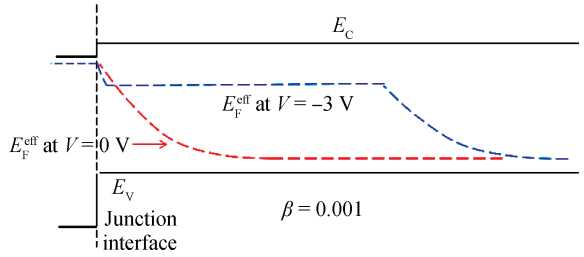


Figure 14. Effective Fermi level of $n^+/p$ junction steady state 1 ($V = 0$) and 2 ($V = -3$ V), $\beta = 0.001$.

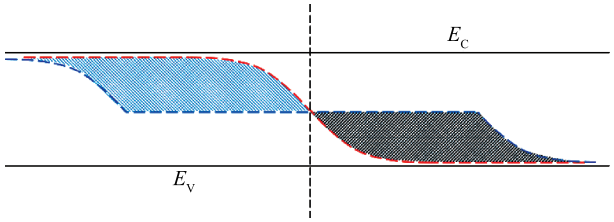


Figure 15. (Color online) Detectable regions of defect TFEL ($\beta = 1$) in a symmetric n/p junction: upper left—electron level EL, lower right—hole level HL.

It is shown in Figure 15 (symmetric n–p junction) and 16 (abrupt $n^+$–p junction) that the defect changes its occupation only when the coordinate $(x, G)$ of the defect TFEL is in the shadowed area. In the lower right:

$$E_{Fn} - E_i \ll G - E_i \sim E_i - E_{Fp} \ll E_i - G,$$
$$\therefore c_n \ll e_n \sim c_p \ll e_p. \tag{18}$$

and in the upper left:

$$E_i - E_{Fp} \ll E_i - G \sim E_{Fn} - E_i \ll G - E_i,$$
$$\therefore c_p \ll e_p \sim c_n \ll e_n. \tag{19}$$

In Figures 15 and 16 it is assumed that $\beta = 1$. For $\beta \neq 1$, the intrinsic Fermi level $E_i$ must be effectively substituted by $E_i + \Delta E_\beta$, shifting by $\Delta E_\beta$ up or down. The dependence of $\Delta E_\beta$ on $\beta$ at 300 K is listed in Table 1.

Apparently in DLTS the SCR charge variation is dominated by hole emission from hole levels (HL) and electron emission from electron levels (EL). In SCR defect characterization, hole emission from HL and electron emission from EL are observed in DLTS when the TFEL $G$ of the HL and EL obey the four rules of selection:

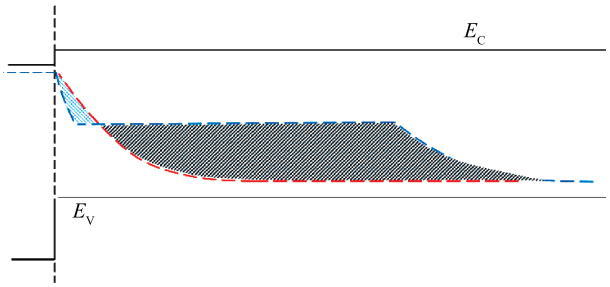


Figure 16. Detectable regions of defect TFEL ($\beta = 1$) in an abrupt $n^+/p$ junction: upper left—electron level EL, lower right—hole level HL.

Selection Rule No. 1: $G_H > E_{Fp}; G_E < E_{Fn}$ (Note: $E_{Fp}$ and $E_{Fn}$ are the quasi Fermi levels of steady state 1 with a small bias voltage. $E_{Fp} = E_{Fn} = E_F$ with no bias. TFEL of the HL and EL $G$ = const, while $E_{Fp}$, $E_{Fn}$, and $E_F$ depend on the location within the SCR.)

Selection Rule No. 2: For symmetric n–p junction, HL detected are mainly in the p-material with $G$ in the lower half of the bandgap, while EL detected are mainly in the n-material with $G$ in the upper half of the bandgap. For abrupt $n^+$–p junction, HL detected are mainly in the p-material away from the interface $n^+/p$ interface, with $G$ in the lower half of the bandgap, while EL detected are mainly in the p-material adjacent to the interface with $G$ in the upper half of the bandgap.

Selection Rule No. 3: HL may be acceptor or double acceptor; it may also be donor or double donor. The hole emission rate of acceptor or double acceptor is higher than that of the donor or double donor. EL may be donor or double donor; it may also be acceptor or double acceptor. The electron emission rate of donor or double donor is higher than that of the acceptor or double acceptor.

(Note: $\sigma_p^{AA} > \sigma_p^A > \sigma_p^D > \sigma_p^{DD}$ and $\sigma_n^{DD} > \sigma_n^D > \sigma_n^A > \sigma_n^{AA}$ due to Coulomb attraction or repulsion between the carrier and the defect.)

Selection Rule No. 4: Signal of hole and electron emission are from HL and EL with $\beta$ located within:

$$\begin{cases} W_H(V_1, V_2; G) = x_{H2}(V_2, G) - x_{H1}(V_1, G), \\ W_E(V_1, V_2; G) = x_{E1}(V_1, G) - x_{E2}(V_2, G), \end{cases}$$
$$< \text{SCR width } W, \text{ with } \begin{cases} G < E_i - \Delta E_\beta, \\ G > E_i - \Delta E_\beta. \end{cases} \tag{20}$$

Note that the dependence of $x_{H2}$, $x_{H1}$, $x_{E1}$, and $x_{E2}$ on $V_2$ ($V_1 \sim 0$) and $G$ as shown in Equation (19) is the essence of spatial dependence of deep level transient spectroscopy (SSLTS). Equation (19) is shown in Figure 16 graphically for symmetric and abrupt junction, respectively, under the condition of $\beta = 1$. For $\beta \neq 1$, similar graphical display of spatial sensitivity of DLTS signals can be plotted as well. For the convenience of application of SSDLTS, by using the band bending parabola profile:

Table 1. Dependence of $\Delta E_\beta$ on $\beta$.

| $\beta$ | $10^{-5}$ | $10^{-3}$ | 0.1 | 1 | 10 | $10^3$ | $10^5$ |
|---|---|---|---|---|---|---|---|
| $\Delta E_\beta$ (eV) | –0.298 | –0.179 | –0.0596 | 0 | 0.0596 | 0.179 | 0.298 |

Table 2. Majority carrier trap (HL, above $E_V$) and minority carrier trap (EL, below $E_C$) experimentally detected by DLTS in comparison of the prediction of this work.

| Parameter | This work | Abufoltu *et al.*[22] | Balcioglu *et al.*[23] | Wang *et al.*[24] | Li *et al.*[25] | Cheng[26] |
|---|---|---|---|---|---|---|
| HL($E_V$+) (eV) | > 0.3 | 0.38 | 0.35 | 0.128 | 0.341, 0.226 | 0.30 |
| EL($E_C$−) (eV) | > 0.1 | 0.59 | | 0.17 | 0.147 | 0.12 |

Symmetric n–p with $W = W_n + W_p$:

$$\Psi(x) = \begin{cases} \dfrac{qN_D}{2\varepsilon}\left[(W_n + x)^2 - W_n^2\right], & -W_n < x < 0, \\ \dfrac{qN_A}{2\varepsilon}\left[W_p^2 - (W_p - x)^2\right], & 0 < x < W_p, \end{cases}$$

Abrupt $n^+$:

$$\Psi(x) = -\frac{qN_A(W - x)^2}{2\varepsilon}, \quad 0 < x < W.$$

Numerical tables can be tabulated for the dependence of $x_{H2}$, $x_{H1}$, $x_{E1}$, and $x_{E2}$ on $V_1$, $V_2$, $G$, and $\beta$.

## 6. Comparison of experimental data with DLTSDP theory

A survey of the published DLTS data of the CdS/CdTe thin film solar cell is listed in Table 2.

## 7. Discussion

It is interesting and important to note:

(1) The reported DLTS experimental data refer to the majority carrier hole trap HL and the minority carrier electron trap El as the defect energy level or transition energy level (TEL) $E$. As discussed in this work they should be called the transition free energy level (TFEL) $G$, which may be quite different from TEL[2, 7].

(2) There is just one hole trap level HL reported by the same group — Wang *et al.*[24] and Li *et al.*[25] that violates the Selection Rule presented in this work. The p-doping level of the CdS/CdTe solar cell junction is low, its quasi Fermi level $E_{Fp}$ is ∼0.3 eV above $E_V$. According to the Selection Rule No.1, no HL less than 0.3 eV can be detected by DLTS. We had also observed such a false HL deep level before it was found to be due to the error in interpreting the data.

(3) The data of defect energy or free energy level extracted from DLTS depends on the temperature. The HL 0.128 eV listed in Table 2[20] is measured at higher temperature (280 K) than usual. The level reported may also be due to some other emission mechanism, for example, from charged defects at the interface.

(4) As shown by References [24, 25] of the same research group, different growth condition may cause different deep levels.

(5) The comparison of reported experimental DLTS data with the theory presented in this work is limited to the energy levels of HL and EL. The data on deep level concentration and cross section will be discussed after more experimental work is performed in the future.

Considering the complexity of DLTS measurement and CdS/CdTe junction processing, the agreement of the reported experimental data and the DLTSDP theory predicted rules is satisfactory.

## Acknowledgment

The authors acknowledge the China Triumph International Engineering Company (CTIEC), Shanghai, China, which offered generous financial support for this work. They also thank Yiming Ding of NJIT and Dr. Suhuai Wei of NREL for helpful discussions and technical support.

## References

[1] Lang D V. Deep-level transient spectroscopy: a new method to characterize traps in semiconductors. J Appl Phys, 1974, 45: 3023

[2] Henry C H, Lang D V. Nonradiative capture and recombination by multiphonon emission in GaAs and GaP. Phys Rev B, 1977, 15: 989

[3] Orton J W, Blood P. The electrical characterization of semiconductors: measurement of minority carrier properties. Academic Press, 1990

[4] Dhere R G, Zhang Y, Romero M J, et al. Investigation of junction properties of CdS/CdTe solar cells and their correlation to device properties. Proceedings of 33rd IEEE PVSC, San Diego, CA, May 2008: 1

[5] Delahoy A E, Cheng Z, Chin K K. Evidence for $CdTe_{1-x}S_x$ compound formation in CdTe solar cells from high-precision, temperature-dependent device measurements. Proceedings of 39th IEEE PVSC, Tampa, FL, June 2013: 1945

[6] Delahoy A E, Cheng Z, Chin K K, et al. Modulation spectroscopy as a probe of surface electric field. Proceedings of 29th EU SEC, Amsterdam, September 2014: 1860

[7] Chin K K. Transition Gibbs free energy level cross section and formulation of carrier SRH recombination rate. Journal of Semiconductors, 2013, 34(12): 122001

[8] Wei S H, Zhang S B. Chemical trends of defect formation and doping limit in II–VI semiconductors: the case of CdTe. Phys Rev B, 2002, 66: 15521

[9] Ma J, Wei S H, Gessert T A, et al. Carrier density and compensation in semiconductors with multi dopants and multi transition energy levels: the case of Cu impurity in CdTe. Phys Rev B, 2011, 83: 245207

[10] Sze S. Physics of semiconductor devices. 2nd ed. New York: Wiley, 1981

[11] Crandall R S. Meyer-Neldel rule in deep-level-transient-spectroscopy and its ramifications. Proceedings of MRS Symposium, San Francisco, April 2003: 79
[12] Yelon A, Movaghar B, Crandall R S. Multi-excitation entropy: its role in thermodynamics and kinetics. Reports on Progress in Physics, 2006, 69: 1145
[13] Chin K K. p-doping limit and donor compensation in CdTe polycrystalline thin film solar cells. Solar Energy Materials and Solar Cells, 2010, 94: 1627
[14] Chin K K. Approximate graphical method for solving Fermi level and majority carrier density of semiconductors with multiple donors and multiple acceptors. Journal of Semiconductors, 2011, 32(6): 062001
[15] Chin K K. Local charge neutrality condition, Fermi level, and majority carrier density of semiconductor with multiple localized multi-Level intrinsic/impurity Defects. Journal of Semiconductors, 2011, 32(11): 112001
[16] Chin K K. Dual roles of doping and trapping of semiconductor defect levels and their ramification to thin film photovoltaics. J Appl Phys, 2012, 111: 104509
[17] Cao W. Analytical formulas for carrier density and Fermi energy in semiconductors with a tight-binding band. Journal of Semiconductors, 2015, 36(4): 042002
[18] Chandra S T, Balamurugan N B, Bhuvaneswari M, et al. Analysis of charge density and Fermi level of AlInSb/InSb single-gate high electron mobility transistor. Journal of Semiconductors, 2015, 36(6): 064003
[19] Cheng Z. Applications of defect level steady state occupation equation in CdTe solar cell. PhD Dissertation, NJIT, 2014
[20] Cheng Z, Delahoy A E, Su Z, et al. Steady state minority carrier lifetime and defect level occupation in thin film CdTe solar cells. Thin Solid Films, 2014, 558: 391
[21] Manual for AMPS-1D, the center for nanotechnology education and utilization, the Pennsylvania State University, 2003
[22] Abulfotuh F A, Balcioglu A, Wangensteen T, et al. Study of the defect levels, electrooptics, and interface properties of polycrystalline CdTe and CdS thin films and their junction. Proceedings of 27th IEEE PVSC, Anaheim, CA, Sep 1997: 451
[23] Balcioglu A, Ahrenkiel R K, Hasoon F. Deep-level impurities in CdTe/CdS thin-film solar cells. J Appl Phys, 2000, 88: 7175
[24] Wang Z, Li B, Zheng X, et al. Deep level transient spectroscopy investigation of deep levels in CdS/CdTe thin film solar cells with Te:Cu back contact. Chinese Physics B, 2010, 19: 027303
[25] Li B, Feng L H, Wang Z, et al. Electronic properties and deep level transient spectroscopy of CdS/CdTe thin film solar cells. Chinese Physics B, 2011, 20: 037103